Slow Photoelectron Spectroscopy of δ-Valerolactam and Its Dimer

ARTICLE *in* CHEMPHYSCHEM · JULY 2011

Impact Factor: 3.42 · DOI: 10.1002/cphc.201100090 · Source: PubMed

10 AUTHORS, INCLUDING:

Ahmed Mahjoub
NASA
42 PUBLICATIONS **146** CITATIONS
SEE PROFILE

Majdi Hochlaf
Université Paris-Est Marne-la-Vallée
240 PUBLICATIONS **1,592** CITATIONS
SEE PROFILE

Lionel Poisson
French National Centre for Scientific Resea…
106 PUBLICATIONS **929** CITATIONS
SEE PROFILE

Laurent Nahon
SOLEIL synchrotron
233 PUBLICATIONS **2,475** CITATIONS
SEE PROFILE

CHEMPHYSCHEM

DOI: 10.1002/cphc.201100090

Slow Photoelectron Spectroscopy of δ-Valerolactam and Its Dimer

Ahmed Mahjoub,[a] Majdi Hochlaf,*[a] Lionel Poisson,[b] Nicolas Nieuwjaer,[c] Frédéric Lecomte,[c] Jean-Pierre Schermann,[c] Gilles Grégoire,[c] Bruno Manil,[c] Gustavo A. Garcia,[d] and Laurent Nahon[d]

We studied the single-photon ionization of gas-phase δ-valerolactam (piperidin-2-one) and of its dimer using vacuum-ultraviolet (VUV) synchrotron radiation coupled to a velocity map imaging electron/ion coincidence spectrometer. The slow photoelectron spectrum (SPES) of the monomer is dominated by the vibrational transitions to the $\tilde{X}$ state. Moreover, several weaker and complex bands are observed, corresponding to the population of the vibrational bands (pure or combination) of the electronically excited states of the cation arising from their mutual vibronic interactions. For the dimer, we measure a unique large band. These spectra are assigned with the help of theoretical calculations dealing with the equilibrium geometries, electronic-state patterns and evolutions, harmonic and anharmonic wavenumbers of the monomer and dimer, either neutral or positively charged. The state energies of the [δ-valerolactam]$^+$ cation in the $\tilde{X}$ ground, $\tilde{A}$, $\tilde{B}$ and $\tilde{C}$ excited electronic states, and of the [δ-valerolactam]$_2^+$ cation's lowest states are determined. After its formation, [δ-valerolactam]$_2^+$ is subject to intramolecular isomerization, H transfer and then unimolecular fragmentation processes. Close to the ionization thresholds, the photoionization of these molecules is found to be mainly dominated by a direct process whereas the indirect route (autoionization) contributes at higher energies.

1. Introduction

Cyclic lactams, such as δ-valerolactam (piperidin-2-one), are important for applied and fundamental purposes. In biology, δ-valerolactam is known to be an inhibitor of alcohol metabolism in primates.[1] Moreover, cyclic lactams are considered as prototype molecules for cyclic peptides. In an industrial context, piperidin-2-one is employed as a monomer to produce nylon-5. Its isomer, piperidin-4-one, is used as an intermediate in the manufacture of chemicals and pharmaceutical drugs (e.g. fentanyl).[2] Finally, the cyclic lactam dimers, which are formed by hydrogen bonding, represent simple models for the hydrogen bonding peptide linkage, which participates into the 3D structural properties of large peptides and proteins. In addition, there are structural similarities between δ-valerolactam (saturated CC bonds) and 2-pyridone (aromatic six-ring cycle) and dimer, which is considered as a simple model for studying the pairing (hydrogen bonding) between DNA basis pairs. This is because they present a small number of hydrogen bonding donor-acceptor sites. In that context, δ-valerolactam represents an even simpler model since only the amide form predominates under laboratory conditions, whereas 2-pyridone possesses two tautomers: a lactam form for 2-pyridone (keto) and a lactim form for 2-hydroxypyridine (enol) which are almost isoenergetic in gas, liquid, and solid phases.[3]

Several structural and spectroscopic studies were performed on the neutral δ-valerolactam molecule. In the 1970s, Warshel et al.[4] and Rey-Lafon et al.[5] analyzed the vibrational structure of this molecule in CCl_4. They derived the force field for this molecule, and pointed out the characteristics of the *cis* and *trans* amide group vibrations. Later on, the equilibrium molecular conformation was reinvestigated and precisely determined after analysis of the microwave spectrum of δ-valerolactam in the gas phase.[6] A chair form is definitely established for this lactam, in accordance with modified neglect of diatomic overlap (MNDO) semi-empirical and ab initio theoretical results at the HF/3-21G, MP2/6-31G(d,p), DFT/B3PW91/6-311++G** and MP2/6-311++G** levels of theory.[6–9]

The molecular structure of the δ-valerolactam$_2$ dimer was characterized using IR, NMR and Raman spectroscopies and theoretical ab initio treatments.[10–16] These works proved the C_2 symmetry of the cyclic hydrogen-bonded dimer (denoted in

[a] *Dr. A. Mahjoub, Prof. Dr. M. Hochlaf*
Université Paris-Est, Laboratoire Modélisation et Simulation Multi Echelle, MSME UMR 8208 CNRS
5 bd Descartes, 77454 Marne-la-Vallée (France)
Fax: (+33) 160957320
E-mail: hochlaf@univ-mlv.fr

[b] *Priv.-Doz. Dr. L. Poisson*
Laboratoire FrancisPerrin, CNRS URA 2453, CEA, IRAMIS
Service des Photons Atomes et Molécules
Bât 522, F-91191 Gif/Yvette (France)

[c] *Dr. N. Nieuwjaer, Dr. F. Lecomte, Prof. Dr. J.-P. Schermann, Priv.-Doz. Dr. G. Grégoire, Prof. Dr. B. Manil*
Laboratoire de Physique des Lasers, CNRS UMR 7538
Institut Galilée, Université Paris
13, 93430 Villetaneuse (France)

[d] *Dr. G. A. Garcia, Priv.-Doz. Dr. L. Nahon*
Synchrotron SOLEIL, L'orme des Merisiers
Saint-Aubin—BP 48, 91192 Gif-sur-Yvette Cedex (France)

Supporting information for this article is available on the WWW under http://dx.doi.org/10.1002/cphc.201100090.

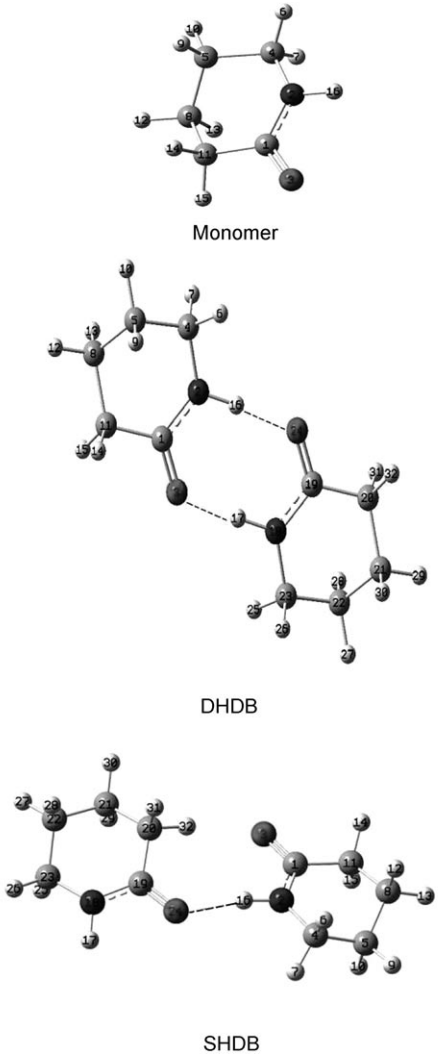

Figure 1. Numbering of the atoms of δ-valerolactam (Table 1) and of its dimers (Table 5).

Figure 1 as DHDB) and determined the equilibrium constants for its formation as a function of the temperature. Specifically, they concentrated on the intermolecular vibration involving the hydrogen bonds of the DHDB. In 2010, the existence of such form was confirmed by means of FTIR and DFT/B3PW91/6-311++G** and MP2/6-311++G** by Pandey et al.[9] In addition, these authors trapped, in a cooled N_2 matrix (~10 K), and identified a less stable form of this dimer where the bonding between the two monomers is ensured by a unique single hydrogen bond (denoted as SHDB, Figure 1).

In contrast to the neutral δ-valerolactam and δ-valerolactam$_2$ molecules, very few is known on their positively charged ions, [δ-valerolactam]$^+$ and [δ-valerolactam]$_2^+$. For the monomer, we can mention the earlier He I photoelectron study by Potapov et al.,[17] and the electronic structure and conformational properties investigations by Treschanke and Rademacher.[7,18] These authors determined the ionization energies (IEs) of δ-valerolactam, at 9.15±0.02 and 9.30 eV, respectively. Their photoelectron spectrum is composed by well-resolved bands, extending over ~1 eV each, that were attributed to the ionization from π_N, n_O for the first two ones and to the inner shell valence ionization for the upper ones. Nothing is known, however, concerning the single positively charged dimer of valerolactam.

The present combined theoretical and experimental work concerns the spectroscopy of the cationic forms of δ-valerolactam and δ-valerolactam$_2$. The ions are formed after vacuum-ultraviolet (VUV) photoionization of the jet-cooled corresponding neutral molecules. The slow photoelectron spectra (SPES) present rich structures corresponding to the population of rovibrational levels of the [δ-valerolactam]$^+$ and [δ-valerolactam]$_2^+$. The assignment of these spectra is based on theoretical calculations on the structures, vibrational wavenumbers and electronic excitation energies of [δ-valerolactam]$^+$ and of [δ-valerolactam]$_2^+$.

Experimental and Computational Methods

Experimental Details: The monochromatized VUV ionizing radiation was delivered by the DESIRS beamline,[19] at the third-generation French synchrotron facility SOLEIL located in St Aubin, France. For this experiment we used a moderate resolution/high flux 200 gr mm^{-1} grating, giving a typical bandwidth of about 2.5 meV. The photon flux was monitored and normalized owing to a VUV Photodiode (IRD AXUV100). The beamline was also equipped with a gas filter,[20] which was filled with Kr to remove the contribution of second-order light and provide a high spectral purity, which is critical for this type of experiment. An additional advantage is that the 5s and 5s′ absorption lines from the Kr[21] in the filter were used to calibrate the energy scale with a precision of ±3 meV. The spectrometer employed herein, DELICIOUS II, has been described in detail elsewhere.[22] Briefly, the electrons and ions are extracted in opposite directions towards a velocity map imaging (VMI)[23] and a Wiley-McLaren time of flight (TOF) spectrometer, respectively, where they are recorded in coincidence. Thus, photoelectron images can be obtained for a particular mass. Herein, the extraction field was set to 19 V cm^{-1}, a value optimized to record threshold electrons with an absolute resolution down to ~9 meV. With this extraction field we expect a 100% collection efficiency for electrons possessing kinetic energies below 190 meV. We have corrected our IEs because of the red-shift of 3 meV DC extraction field. For more details about our experimental methodology, and especially the extraction of SPES, we refer to our recent work on 2-pyridone and of its tautomer.[24]

A commercial sample of δ-valerolactam (purchased from Sigma–Aldrich with 97% purity) was placed in an in-vacuum temperature-controlled oven installed inside the SAPHIRS molecular beam chamber. The oven was heated to 130 °C. The resulting vapor was mixed with 0.5 bar of He and expanded through a 50 μm nozzle into a first (expansion) chamber maintained at 1.2×10^{-5} mbar. The supersonic beam then entered a second ionization chamber through a 1 mm skimmer where it crosses the photon beam at a right angle in the centre of the DELICIOUS II spectrometer. The jet conditions (carrier gas, backing pressure, oven temperature) were optimized to produce mainly the monomer and the dimer of δ-valerolactam. As mentioned above, the photoelectron images were correlated to the ion mass-to-charge ratio, allowing us to filter out the contributions of the parent monomer or the parent dimer or their fragments to the photoelectron spectra. For such studies, it is crucial to make sure that the monomer and dimer channels are decoupled, that is, that dissociative ionization processes of the dimer do not give any contribution to the monomer channel. This decou-

pling was carefully checked by mass-selected ion imaging on the monomer mass, and in the photon energy covered herein, we did not see any kinetic-energy release (KER) for the monomer ion. Therefore the *mass* selection that we can achieve by mass spectrometry does correspond to the *size* selection of the nascent monomer or dimer species in the jet. Therefore, the spectra discussed below concern pure monomeric or dimeric species.

Computational Details: Electronic-structure calculations were performed using the MOLPRO and GAUSSIAN packages.[25,26] In these calculations, we were interested in determining: i) the equilibrium molecular structures of the neutral and cationic monomer and dimer in their respective electronic ground states; and ii) the pattern of the lowest electronic states of the singly charged species. Our calculations were carried out in the C_1 point group symmetry. In these calculations, two basis sets were used for the description of the hydrogen, carbon, nitrogen and oxygen atoms: the aug-cc-pVDZ basis set and the aug-cc-pVTZ of Dunning and co-workers.[27,28] The aug-cc-pVDZ basis set results in 242 and 484 contracted Gaussian functions (GTO) to be considered for the monomer and dimer, respectively. The aug-cc-pVTZ basis set leads to 242 and 529 GTOs for the monomer and dimer, respectively, to be treated.

For the equilibrium molecular-structure optimizations, we used the aug-cc-pVDZ basis set, the PBE0 exchange-correlation functional[29] and the standard options, as implemented in the Gaussian code.[30] Further on, the optimizations were performed at the MP2/aug-cc-pVTZ level for better accuracy.

For the mapping of the electronic states of [δ-valerolactam]$^+$ and [δ-valerolactam]$^{2+}$, we used a fully ab initio methodology and a time-dependant density functional theory (TD-DFT) approach. In the TD-DFT calculations, only the smaller basis set, aug-cc-pVDZ, was used. In ref. [31], we showed that this is enough for direct comparison with ab initio data.

The ab initio calculations start with restricted Hartree–Fock (RHF) calculations on the electronic ground state of [δ-valerolactam]$^+$ or of [δ-valerolactam]$_2^+$. Then, we performed a complete active-space self-consistent field (CASSCF)[32,33] study followed by internally contracted multi-reference configuration interaction (MRCI) computations.[34,35] Both methods are implemented in the MOLPRO program suite.[25] In CASSCF, the electronic states were averaged together with equal weights using the MOLPRO state averaging procedure. With the available MOLPRO versions, we cannot consider all valence molecular orbitals of the monomer or of the dimer in the active space. Hence, we did several tests to reduce the size of the active space without disturbing strongly the pattern of the [δ-valerolactam]$^+$ and of the [δ-valerolactam]$_2^+$ doublets located in the 0–5 eV internal energy domain. For the monomer, the best compromise (calculation costs and accuracy) is for an active space comprising all the molecular orbitals (MOs) from HOMO-16 to LUMO+3 as active (HOMO: highest occupied molecular orbital; LUMO: lowest unoccupied molecular orbital). The HOMO-1 to HOMO-15 MOs are frozen. For the dimer, we choose an active space considering the HOMO-6 to LUMO+4 as active. Then, the resulting active spaces are constructed using all configuration state functions (CSFs) obtained after excitations of all valence electrons in these orbitals. For the monomer (dimer) cation calculations, we treated hence $\sim 3\times10^5$ ($\sim 2.8\times10^4$) CSFs. At the MRCI level of theory, all configurations with coefficients larger than 0.5 in the CI expansion of the CASSCF wavefunctions were taken as reference, and all electrons were correlated. For the ionic monomer, this leads to more than 8.7×10^7 uncontracted configurations to be treated.

2. Spectroscopy of the [δ-Valerolactam]$^+$ Cation

a. Theoretical Results

δ-Valerolactam is dominantly described by the $(22a)^2(23a)^2(24a)^2(25a)^2(26a)^2(27a)^2$ electron configuration. Table 1 lists the DFT PBE0/aug-cc-pVDZ equilibrium molecular structure of δ-Valerolactam and of its cation in their electronic ground states. The numbering of the atoms is given in Figure 1. Both the neutral δ-valerolactam and the [δ-valerolactam]$^+$ ion present no symmetry (belong to the C_1 point group). Inspection of the equilibrium geometrical differences between the ionic and their neutral parent species shows that only slight geometrical changes are occurring upon photoionization of δ-valerolactam. Table 1 shows that the main changes are for the C_1-N_2, C_1-C_{11}, C_1-O_3 distances, O_3-C_1-N_2 in-plane angle and the C_{11}-C_1-N_2-C_4,

Table 1. Equilibrium molecular structure of δ-valerolactam and its cation in their respective electronic ground states. These parameters are computed at the DFT PBE0/aug-cc-pVDZ level of theory. Distances are in pm and angles in degrees. See Figure 1 for the atom numbering.

	δ-Valerolactam	δ-Valerolactam$^+$		δ-Valerolactam	δ-Valerolactam$^+$
N_2–H_{16}	101.1	102.3	C_{11}–C_1–N_2–C_4	26.3	29.2
C_1–N_2	136.3	123.5	C_1–N_2–C_4–C_5	26.3	29.2
C_1–O_3	122.4	123.5	N_2–C_4–C_5–C_8	49.8	46.4
C_1–C_{11}	151.5	149.3	C_4–C_5–C_8–C_{11}	61.0	58.1
C_{11}–C_8	152.4	153	C_5–C_8–C_{11}–C_1	46.0	49.0
C_8–C_5	152.2	152.5	C_8–C_{11}–C_1–N_2	21.2	31.2
C_5–C_4	151.9	151.6	C_1–N_2–C_4–H_{16}	165.9	159.7
C_4–N_2	145.3	144.6	C_5–C_4–N_2–H_7	121.4	124.2
C_5–H_9	110.1	109.9	C_5–C_4–N_2–H_6	121.6	123.9
C_5–H_{10}	109.8	109.6	C_4–C_5–C_8–H_{10}	120.6	120.3
C_4–H_7	110.4	110.8	C_4–C_5–C_8–H_9	120.6	121.4
C_4–H_6	109.9	110.3	C_5–C_8–C_{11}–H_{12}	122.5	121.2
C_8–H_{12}	109.8	109.6	C_5–C_8–C_{11}–H_{13}	120.3	122.2
C_8–H_{13}	110.1	109.9	C_8–C_{11}–C_1–H_{15}	125.2	125.1
C_{11}–H_{15}	109.6	109.5	C_8–C_{11}–C_1–H_{14}	121.8	120.5
C_{11}–H_{14}	110.1	110.3	C_{11}–C_1–N_2–O_3	177.4	176.1
C_1–N_2–H_{16}	113.3	114.2	C_8–C_{11}–C_1–O_3	158.7	171.7
O_3–C_1–N_2	121.2	113.8			
C_4–N_2–C_1	127.0	123.9			
N_2–C_1–C_{11}	117.0	119.8			
C_1–C_{11}–C_8	114.7	111.5			
C_{11}–C_8–C_5	109.9	110.8			
C_8–C_5–C_4	109.9	111.3			
C_5–C_4–N_2	111.1	112.1			

C_8-C_{11}-C_1-N_2, C_1-N_2-C_4-H_{16} and C_8-C_{11}-C_1-O_3 dihedral angles. Indeed, the C_1-N_2, C_1-C_{11}, C_1-O_3 distances are longer and these angles are varying by ~10° upon ionization of this molecule. For the neutral molecule, our geometrical parameters compare quite well with those determined through the microwave study of Kuze et al.[6] and those computed recently by Pandey et al.[9]

We display in Table 3 the harmonic and anharmonic wavenumbers (in cm^{-1}) of the 42 vibrational modes of δ-valerolactam$^+$ in its electronic ground state. These data are computed at the PBE0/aug-ccpVDZ level and using the standard options as implemented in Gaussian.[26] In other words, this consists on the calculations of the derivatives of the potential energy surface (PES) at the minimum equilibrium molecular structure and on the application of second order perturbation theory. For the low frequency modes, strong anharmonic behaviors were noticed invalidating the use of perturbation theory for them. They mainly concern the out-of-plane torsion modes for which the PESs strongly vary along the corresponding coordinates.

The electronic ground state $\tilde{X}^2A$ of the [δ-valerolactam]$^+$ cation is obtained after removal of one electron from the outermost (27a) MO. The electronic excited states $\tilde{A}^2A$ and $\tilde{B}^2A$ of the cation are obtained after ejection of one electron from the (26a) and (25a) MOs of δ-valerolactam, respectively (cf. Table 4). The electronic wavefunctions of the $\tilde{C}^2A$ and $\tilde{D}^2A$ states present strong multiconfigurational characters [(23a) and (24a) MOs]. At the MRCI + Q/CASSCF/aug-cc-pVDZ level of theory, the $\tilde{A}^2A$, $\tilde{B}^2A$, $\tilde{C}^2A$ and $\tilde{D}^2A$ states are computed to lie at 0.52, 2.90, 3.22 and 3.55 eV with respect to the [δ-Valerolactam]$^+$ $\tilde{X}^2A$ energy at equilibrium. Table 4 lists also the vertical excitation energies of this cation computed at the PBE0/aug-cc-pVDZ, CASSCF/aug-cc-pVDZ, CASSCF/aug-cc-pVTZ levels of theory. After examination of these data, several remarks can be drown: i) the smaller basis set is large enough to study the positively charged species since the larger aug-cc-pVTZ basis set leads to similar data as those obtained by the aug-cc-pVDZ basis; ii) TD-DFT reproduces quite well the electronic spectrum of this cation. It is therefore, an accurate enough alternative for the deduction of the pattern of the electronic states of ionized molecules close to equilibrium; iii) the inclusion of dynamical correlation (in MRCI) seems not to strongly affect the pattern of these electronic states. Hence, the CASSCF level is enough to map their potential energy surfaces far from equilibrium.

From the PE spectrum of Treschanke and Rademacher,[18] one may determine the ionization energies of the four lowest electronic states of [δ-valerolactam]$^+$, at 0.5, 2.1, 2.8 and 3.0 eV, with respect to the ground state origin band of the cation. These energies correspond to the vertical ionization process. They compare quite well to those computed presently (Table 4). The unresolved nature of the bands recorded by these authors is most likely due to the congestion of these spectra because of unfavorable Franck–Condon factors upon ionization (leading to their formation) and/or due to their mutual vibronic couplings (see below).

The upper panel in Figure 4 depicts the CASSCF/aug-cc-pVDZ one-dimensional evolutions of the potential energy surfaces of the lowest doublet electronic states of [valerolactam]$^+$ along the planarization angle θ. The lower panel in Figure 4 displays the one-dimensional evolution of these electronic states along the normal coordinate relative to the out-of-plane torsion 41 mode (Table 3). Figure 4 shows that the ground electronic state $\tilde{X}^2A$ and the first excited state $\tilde{A}^2A$ become close to each other for $\theta \sim 190°$ and $\Delta\tau \sim 14°$ where one can see an avoided crossing along the corresponding coordinates. At these nuclear configurations, both electronic states are coupled vibronically and their electronic wavefunctions are strongly mixed (multiconfigurational nature). Such vibronic interactions strongly disturb the pattern of the rovibrational levels of the $\tilde{X}^2A$ and the $\tilde{A}^2A$ states located in the vicinity of this avoided crossing. Especially, Figure 4 reveals that such couplings take place close to the equilibrium molecular structure of the $\tilde{A}^2A$ state. Therefore, the pattern of the rovibronic levels of this electronic state should be complex and far from conventional. The derivation of the rovibronic spectrum of the $\tilde{A}^2A$ state needs a full variational treatment on a multidimensional PES. This is out of the scope of the present paper. Below, we will confirm experimentally the complexity of the $\tilde{A}^2A$ spectrum.

b. 2D and SPES Spectra

At each photon energy, photoelectron images and the corresponding ions' TOF were recorded in coincidence, so that VMI electron images can be extracted for any particular peak in the mass spectrum. The mass-filtered photoelectron images are later Abel- transformed to recover the original radial (kinetic energy) distributions.[24,36] The polarization vector of the radiation was horizontal to the VMI detector. In the following treatment, we did not observe any polarization in the photoelectron distribution. Hence, we assumed an anisotropy parameter (β) equal to zero for the treatment of the VMI images.

The upper panel of Figure 2 displays the full 2D spectrum of δ-valerolactam in the 8.2–12.5 eV photon energy range and for photoelectrons having kinetic energies from 0 to 190 meV. The parallel lines that one may see on the left-hand side of this figure correspond to different cationic levels populated by direct photoionization, whereas broad unstructured bands can be seen in the middle and right part of this 2D spectrum, which points to autoionization processes occurring at these energies (see below). In summary, the photoionization of δ-valerolactam occurs by direct photoionization in the vicinity of the IE whereas both direct and indirect processes are in action for $h\nu > 9.5$ eV. For instance, we can mention the vibrational autoionization of the neutral states lying just above the cationic bands. In the bottom panel of Figure 2, the slow photoelectron spectrum (SPES) of δ-valerolactam in the 8.2–12.5 eV photon-energy range is shown. This spectrum is obtained by considering the sum signal of photoelectrons having kinetic energies close to zero (up to 75 meV) versus the photon energy. In our recent work on the photoionization of 2-pyridone and its tautomer, we showed that such a summation procedure ensures a much better statistics than the plain threshold photoelectron spectrum (TPES), without strongly affecting the overall resolution.[24]

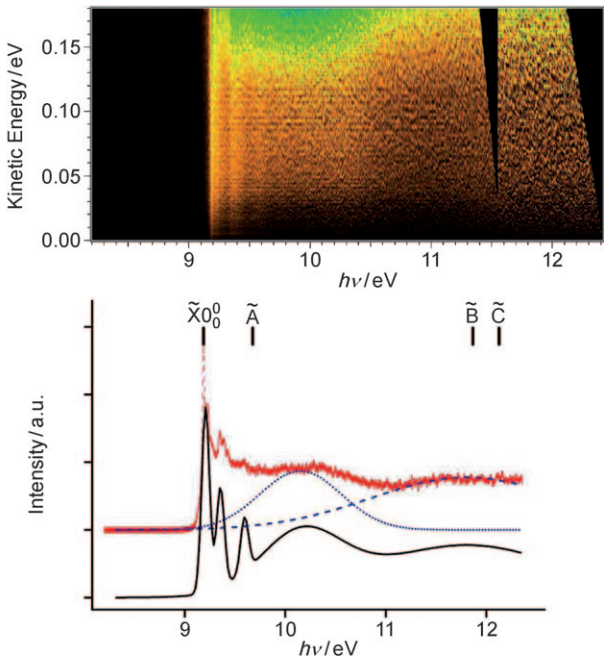

Figure 2. Top: Full-scale 2D spectrum of δ-valerolactam providing the photoelectron kinetic energies as a function of the photon energy after the energy-shifting treatment.[24] Bottom: Slow photoelectron spectrum (SPES) (red line) for electron kinetic energies from 0 to 57 meV as deduced from the 2D spectrum. The positions of the theoretically determined origin transitions are highlighted with vertical bars. The synthetic spectrum is obtained after a rough adjustment of the experimental spectra assuming few Gaussian profiles: the narrow bands at the left side are for the ground state and the larger ones are for the autoionising states. See text for more details.

The SPES spectrum is dominated by the δ-valerolactam $\tilde{X}0_0^0 + h\nu \rightarrow$[δ-valerolactam]$^+$ $\tilde{X}0_0^0 + e^-$ photoionization transition between ground states defining the IE of δ-valerolactam at 9.190 ± 0.003 eV. Our IE is slightly higher than the earlier IE of 9.15 ± 0.02 eV deduced from the photoionization study of Potapov et al.[17] However, our value is distinctly lower (by 0.11 eV) than the value of 9.30 eV determined by Treschanke and Rademacher.[18]

Possible hot bands that would appear on the low-energy side of the origin band $\tilde{X}0_0^0$, are vanishingly weak so that we will neglect them hereafter in the full analysis of our spectrum. Above threshold, several bright vertical lines in the 2D spectrum that correspond to bands in the SPES spectrum are measured. They are due to the population of vibrationally and/or electronically excited states of the singly charged [δ-valerolactam]$^+$ ion.

c. Tentative Assignment of the SPES Spectrum of δ-Valerolactam

All 42 vibrational modes of [δ-valerolactam]$^+$ are—a priori—active by direct photoionization of the corresponding neutral molecule. However, small geometrical changes are observed between the neutral and the ion. Following the Franck–Condon principle, we expect short vibrational progressions upon ionization of δ-valerolactam. This is coherent with the relatively simple shape of the measured experimental SPES spectrum, at least for $h\nu < 10$ eV. The tentative assignment of this SPES spectrum is based on the present theoretical data. Especially, we propose the excitation of some vibrational modes. This is guided by the anharmonic wavenumbers deduced for [δ-valerolactam]$^+$ and the decomposition of the corresponding normal modes on the internal coordinates (Table 3).

In addition to the band origin transition from the neutral species (denoted as $\tilde{X}0_0^0$), some rich vibrational progressions appear. We quote in Table 2 the energies of the maximum of the bands. They are also marked by vertical lines in Figure 3. We are quite confident in our procedure for the isolated bands, whereas this deduction is less accurate for the merging bands. For $h\nu < 9.7$ eV (Figure 3 and Table 2), these bands are attributed to the photoionization transitions populating the [δ-valerolactam]$^+$ $\tilde{X}$ (ground) vibrational levels. Based on the

Table 2. Ionization energies (IE) [eV] of the photoionization bands deduced from the SPES spectrum of Figure 3 (see text). We also give their relative positions (ΔE) [cm^{-1}] with respect to the corresponding electronic ground vibrational levels and their tentative assignment.

Tentative assignment	IE	ΔE	Tentative assignment	IE	ΔE
$\tilde{X}0_0^0$	9.190	0[a]	$\tilde{X}19_0^1 41_0^5$	9.464	2209
$\tilde{X}41_0^1$	9.213	185	$\tilde{X}19_0^1 40_0^4$	9.483	2363
$\tilde{X}41_0^2$	9.236	370	$\tilde{X}19_0^1 31_0^2$	9.503	2524
$\tilde{X}41_0^3$	9.261	572	$\tilde{X}19_0^2$	9.506	2548
$\tilde{X}41_0^4$	9.285	766	$\tilde{X}19_0^2 41_0^1$	9.525	2701
$\tilde{X}41_0^5$	9.303	911	$\tilde{X}19_0^2 40_0^1$	9.534	2774
$\tilde{X}41_0^6$	9.325	1088	$\tilde{X}19_0^2 41_0^2$	9.549	2895
$\tilde{X}19_0^1$	9.355	1330	$\tilde{X}19_0^2 40_0^2$	9.567	3040
$\tilde{X}19_0^1 41_0^1$	9.375	1492	$\tilde{X}19_0^2 41_0^3$	9.574	3096
$\tilde{X}19_0^1 40_0^1$	9.386	1580	$\tilde{X}19_0^2 41_0^4$	9.598	3290
$\tilde{X}19_0^1 41_0^2$	9.399	1685	$\tilde{X}19_0^2 40_0^3$	9.601	3314
$\tilde{X}19_0^1 40_0^2$	9.416	1822	$\tilde{X}19_0^2 41_0^5$	9.617	3443
$\tilde{X}19_0^1 41_0^3$	9.426	1903	$\tilde{X}19_0^2 40_0^4$	9.634	3580
$\tilde{X}19_0^1 31_0^1$[b]	9.433	1959	$\tilde{X}19_0^2 41_0^6$	9.639	3621
$\tilde{X}19_0^1 41_0^4$	9.449	2088	$\tilde{X}19_0^3$	9.659	3782
$\tilde{X}19_0^1 40_0^3$	9.451	2104			

[a] Used as reference. [b] We arbitrarily assign the excitation of this combination mode to the ring-breathing mode. Modes 34 or 35 are also possible, see Table 3.

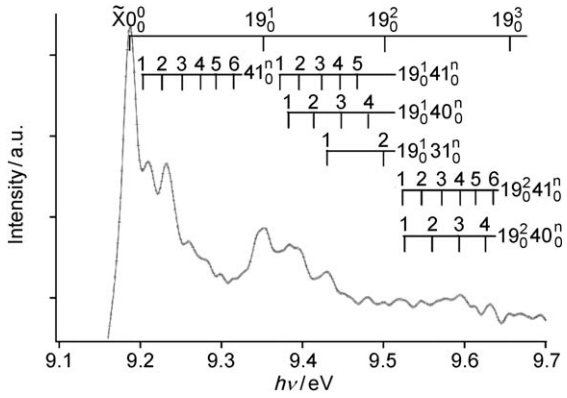

Figure 3. Blow-up of the SPES spectrum of Figure 2 in the regions 9.1–9.7 eV where the vertical lines correspond to our tentative assignments.

PBE0/aug-cc-pVDZ data (Table 3), we fully assign these vibrational features to the pure vibrational progressions or combination modes involving the cationic vibrational modes 19, 31, 40 and 41. The analysis of our spectrum allows the determination of some fundamentals of [δ-Valerolactam]$^+$: $\nu_{19}^+ \sim 1330$, $\nu_{31}^+ \sim 630$, $\nu_{40}^+ = 250$ and $\nu_{41}^+ = 185$. All values are given in cm^{-1}. Note that several assignments can be proposed for the bands involving the mode 31. They are specified in Table 2.

Table 3. Harmonic (ω, in cm^{-1}) and anharmonic wavenumbers (ν, in cm^{-1}) of δ-valerolactam$^+$ in its electronic ground state computed at the PBE0/aug-ccpVDZ level of theory. δ: in-plane angle deformation, τ: out-of plane torsion.

Mode number	ω	ν	Assignment	Mode number	ω	ν	Assignment
1	3506	3384	$\nu(N_2H_{16})$	22	1207	1128	CH_2 twisting
2	3161	3003	CH_2 asym. stretch	23	1138	1135	CH_2 twisting
3	3156	2986	CH_2 asym. stretch	24	1105	1097	ring stretch
4	3152	2985	CH_2 asym. stretch	25	1090	1067	ring stretch
5	3088	2956	CH_2 asym. stretch	26	1066	1021	ring stretch
6	3079	2949	CH_2 sym. stretch	27	978	940	ring breathing
7	3058	2920	CH_2 sym. stretch	28	943	923	ring breathing
8	3052	2924	CH_2 sym. stretch	29	894	791	ring breathing
9	2984	2914	CH_2 sym. stretch	30	877	871	CH_2 rocking
10	1581	1263	$\nu(C_1O_3)$	31	826	662	ring breathing
11	1476	1421	CH_2 scissoring	32	788	752	ring breathing
12	1467	1428	CH_2 scissoring	33	743	721	$\tau(H_{16}N_2C_1C_4)$
13	1448	1434	CH_2 scissoring	34	672	588	ring breathing
14	1422	1373	CH_2 scissoring	35	640	439	ring breathing
15	1397	1388	CH_2 scissoring	36	542	469	$\tau(H_{16}N_2C_1O_3)$
16	1378	1349	CH_2 rocking	37	458	348	$\delta(C_{11}C_8C_5)$
17	1359	1343	CH_2 rocking	38	425	422	ring breathing
18	1346	1312	CH_2 twisting	39	352	–[a]	δ(O3C1N2)
19	1323	1290	ν(C4N2)	40	287	273	ring planarization $\tau(C_5C_8C_1O_3)$
20	1274	1239	CH_2 twisting	41	177	–[a]	$\tau(C_{11}C_8N_2C_4)$
21	1237	1219	CH_2 twisting	42	100	–[a]	$\tau(O_3C_{11}C_1N_2)$

[a] Modes presenting strong anharmonic behavior.

In the 9.7–10.5 eV photon-energy range, the SPES spectrum is more complex. It is composed of several peaks arising from groups of vibrational modes of similar frequencies and most likely progressions of them. These features are superimposed to a non-zero real signal whose origin is explained below. According to the theoretical results, this part of the spectrum should correspond to the photoionization transitions populating the high vibrational levels of the [δ-valerolactam]$^+$ $\tilde{X}^2A$ and those of [δ-valerolactam]$^+$ $\tilde{A}^2A$. As said above, Figure 4B shows that the $\tilde{A}^2A$ state presents a minimum, which is located outside the FC region at least along the 41 normal mode coordinate. Long vibronic progressions are therefore expected for the [δ-valerolactam]$\tilde{X} + h\nu \rightarrow$[δ-valerolactam]$^+$ $\tilde{A}^2A$ photoionization transition, where no distinct origin band can be determined for the $\tilde{A}$ state because of unfavorable Franck–Condon factors. These features seem to be structured. However, we do not have enough signal-to-noise (*S/N*) to be strictly affirmative. Speculatively, we roughly identify several progressions involving four vibrational modes of the $\tilde{A}^2A$ cationic state of the monomer. These modes could correspond to vibrational spacings of ~0.022 eV (~180 cm^{-1}), 0.032 eV (~260 cm^{-1}), 0.157 eV (~1265 cm^{-1}), ~0.250 eV (~2015 cm^{-1}). Based on these wavenumbers, the nature of these modes would be similar to its described in Table 3 for the ground state.

For $h\nu > 11.5$ eV, the SPES spectrum is structure-less because of a congestion of the bands resulting from the ionization of the upper vibrational bands of the $\tilde{X}$ and $\tilde{A}$ states, and because of the population of the $\tilde{B}$ and $\tilde{C}$ states of [δ-valerolactam]$^+$ and the prominent contribution of autoionization and predissociation processes. Based on our theoretical calculation results (Figure 4), the $\tilde{B}$ and $\tilde{C}$ states of the cation should present, similarly to the $\tilde{A}$ state, close-to-zero Franck–Condon factors for the adiabatic transitions. This is because of geometrical changes between the neutral and these ionic states (at least more than 10° for out-of plane angles). Solely the high vibronic bands should be reached and contribute to the spectrum.

Underneath the vibronic structures of the [δ-valerolactam]$^+$ states, there exist two broad profiles (shown as dotted and dashed curves in the SPES spectrum of Figure 2), peaked at about 10.15 and 11.80 eV, respectively. These profiles are fitted Gaussian functions with a full-width-at-half-maximum (FWMH) of $\approx 0.82 \pm 0.1$ eV for the first band and $\approx 1.34 \pm 0.2$ eV for the second band. They may correspond to short-lived neutral states that decay via autoionization into the cationic states populating the complex vibronic bands of the $\tilde{X}$, $\tilde{A}$, $\tilde{B}$ and $\tilde{C}$ states of [δ-valerolactam]$^+$. The 2D spectra of Figure 2 show that these bands are poorly structured. Instead, we observe two large nonzero photoelectron bands. This confirms the autoionization process associated with these bands. Such features were already observed during the photoionization of small and medium sized molecules.[24,37]

3. Spectroscopy of the [δ-Valerolactam]$_2^+$ Cation

a. Theoretical Results

We optimized the equilibrium structures of [δ-valerolactam]$_2$ and [δ-valerolactam]$_2^+$. For the neutral species, two isomers are found (see Figure 1), namely DHBD (for doubly H-bonded dimer) and SHBD (for singly H-bonded dimer), as previously denoted by Pandey et al.[9] (Figure 1). Our PBE0/aug-cc-pVDZ results coincide with those obtained at the DFT/B3PW91/6-311++G(d,p) level of theory by Pandey et al.,[9] except for the

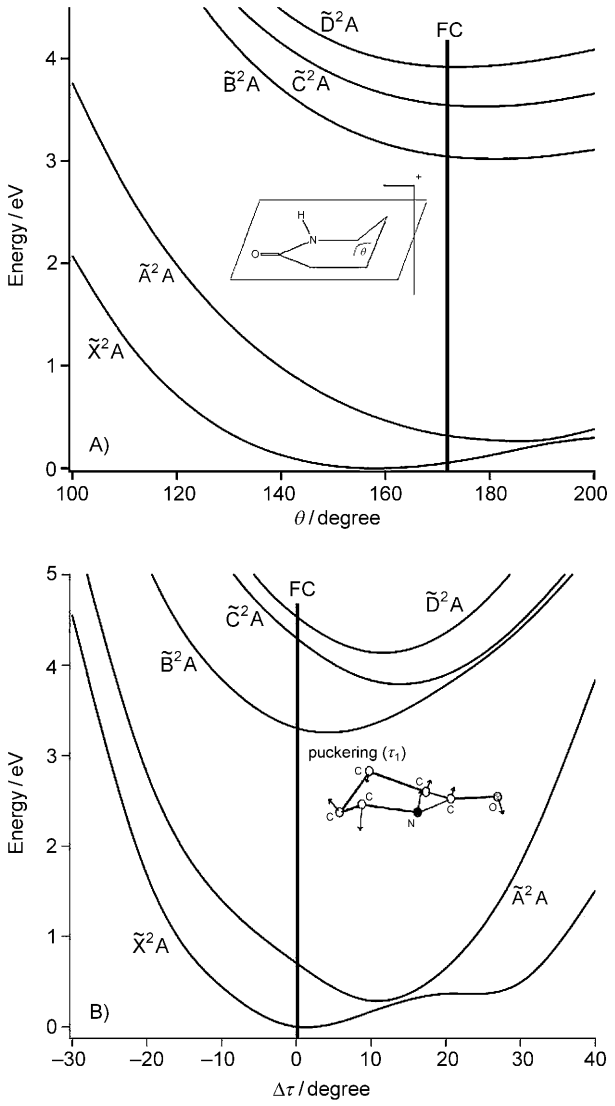

Figure 4. A) CASSCF/aug-cc-pVDZ one-dimensional cuts of the potential energy surfaces of the lowest doublet electronic states of valerolactam$^+$ along the planarization coordinate, θ. The remaining internal coordinates are kept fixed at their equilibrium values in valerolactam$^+$ $\tilde{X}$. B), CASSCF/aug-cc-pVDZ one-dimensional cuts of the potential energy surfaces of the lowest doublet electronic states of valerolactam$^+$ along the normal coordinate, $\Delta\tau$ (mode 41). These curves are given in energy with respect to the energy of valerolactam$^+$ X at equilibrium. The solid thick vertical line corresponds to the middle of the Franck–Condon (FC) region accessible from valerolactam $\tilde{X}$.

O_{24}–H_{16} inter molecular distance. Indeed, differences between both sets of data are less than 0.4 pm for the distances and they are less than 1° for the in-plane angles and out-of-plane torsion angles. In contrast, we compute a distinctly shorter O_{24}–H_{16} distance of 179.2 pm instead of 183.8 pm in their study. DHDB is more stable by about 0.22–0.25 eV.

For the ionic species, we find two isomers, which correspond to the ionized forms of DHBD and SHBD. At the PBE0/aug-cc-pVDZ level, $DHBD^+$, we compute one imaginary wavenumber[38] (i.e. transition state), whereas $SHDB^+$ presents only positive wavenumbers (i.e. equilibrium minimal structure). However, the magnitude of the imaginary wavenumber of $DHDB^+$ is very low ($\sim 8i\,cm^{-1}$) and further treatment at higher levels of theory taking into account larger electronic correlation may correct this fact. The capacity of our available computational resources does not allow larger calculations. Nevertheless, the exact nature of $DHDB^+$ (stable isomer or transition state) is not that crucial since the present theoretical study is mainly devoted to assign the experimental spectra obtained after photoionizing [δ-valerolactm]$_2$ dimer (see below).

The difference in energy between the $DHDB^+$ and $SHDB^+$ structures is ~0.1 eV in favor of$SHDB^+$. After ionizing DHDB, the main geometrical changes (Table 5) occur on the intermolecular part of $DHBD^+$ (i.e. C_1 N_2 H_{16} O_3 and C_{19} N_{18} H_{17} O_{24}, Figure 1): i) the C–N bonds are lengthened by 2 pm; in contrast, the O_{24}-H_{16} bond shrinks by ~9 pm because of the strengthening of the hydrogen bonds upon ionization; ii) this ionization transition is accompanied a C_1-O_3-H_{17} in-plane angle change of ~10°. For the SHBD→$SHBD^+$ ionization transition, we notice similar tendencies. Briefly, the H_{16}–O_{24} increased from 187 to 200 pm and the O_3–O_{24} distance strongly shortens from 377 to 218 pm, together with a reduction of the O_{24}-H_{16}-N_2 in-plane angle from 171° to 126°. At the PBE0/aug-cc-pVDZ, the ionization energies are calculated IE(DHDB) = 8.1 eV and IE-(SHDB) = 7.8 eV.

Table 4 lists the vertical excitation energies of the lowest doublet states of $DHBD^+$. These energies were computed using the PBE0/aug-cc-pVDZ, CASSCF/aug-cc-pVDZ and CASSCF/aug-cc-pVTZ methodologies. They are given in energy with respect to the ground state of $DHBD^+$. Whatever the level of theory used, our calculations lead to a group of 4 electronic states in the 0–1 eV energy range (i.e. the $\tilde{X}$, $\tilde{A}$,$\tilde{B}$ and $\tilde{C}$ states), followed by a gap of states for energies comprised between 1 and 2.4 eV and then the upper doublets are located for energies above 2.4 eV (e.g. the $\tilde{D}$ state).

b. Slow Photoelectron Spectrum of [δ-Valerolactam]$_2$ and Assignment of the Experimental Spectrum

Figure 5 displays the 2D photoelectron map and the SPES spectrum for the photoionization of the [δ-valerolactam]$_2$ dimer. According to the combined matrix FTIR and theoretical studies carried out by Pandey et al.,[9] the bonding in neutral SHBD is weak. They showed also that SHBD is observable only when trapped in cooled N_2 matrices (~10 K). Considering in addition, the 0.22–0.25 eV computed energy difference between the two neutral dimer conformers, we conclude that solely the DHBD form of the dimer should be prominent in our jet molecular beam. The examination of the 2D map reveals that the photoionization of this dimer results in a broad distribution due to unfavorable FC factors, pointing to an important change of geometry between the structures of the ionic and neutral species. Nevertheless, the ionization processes remains mainly direct, since the energy of the electron distribution rises correspondingly to the photon energy.

Figure 5 shows that the SPES spectrum is composed by a unique large band extending from 8.2 to 9.3 eV. According to our theoretical results, this band corresponds to the popula-

Table 4. Dominant electron configurations and excitation energies [eV] of δ-valerolactam$^+$ and of the [δ-valerolactam]$_2^+$ dimer computed at their respective ground-state equilibrium molecular structures.

State	Electron configuration	PBE0/ aug-cc-pVDZ	CASSCF/ aug-cc-pVDZ	MRCI/ CASSCF/aug-cc-pVDZ	CASSCF/ aug-cc-pVTZ	Exp.[a]
		δ-Valerolactam$^+$				
$\tilde{X}^2A$	$(22a)^2(23a)^2(24a)^2(25a)^2(26a)^2(27a)^1$	0[b]	0[b]	0[b]	0[b]	0[b]
$\tilde{A}^2A$	$(22a)^2(23a)^2(24a)^2(25a)^2(26a)^1(27a)^2$	0.57	0.49	0.52	0.50	0.5
$\tilde{B}^2A$	$(22a)^2(23a)^2(24a)^2(25a)^1(26a)^2(27a)^2$	2.46	2.68	2.90	2.59	2.1
$\tilde{C}^2A$	$(22a)^2(23a)^2(24a)^1(25a)^2(26a)^2(27a)^2$ & $(22a)^2(23a)^1(24a)^2(25a)^2(26a)^2(27a)^2$	2.63	2.94	3.22	2.97	2.8
$\tilde{D}^2A$	$(22a)^2(23a)^2(24a)^1(25a)^2(26a)^2(27a)^2$ & $(22a)^2(23a)^1(24a)^2(25a)^2(26a)^2(27a)^2$	2.74	3.40	3.55	3.31	3.0
State		[δ-Valerolactam]$_2^+$ PBE0/ aug-cc-pVDZ	CASSCF/ aug-cc-pVDZ		CASSCF/ aug-cc-pVTZ	
$\tilde{X}^2A$	$(49a)^2(50a)^2(51a)^2(52a)^2(53a)^2(54a)^1$	0[b]	0[b]		0[b]	
$\tilde{A}^2A$	$(49a)^2(50a)^2(51a)^2(52a)^1(53a)^2(54a)^2$	0.24	0.26		0.24	
$\tilde{B}^2A$	$(49a)^2(50a)^2(51a)^2(52a)^2(53a)^1(54a)^2$	0.61	0.45		0.30	
$\tilde{C}^2A$	$(49a)^2(50a)^2(51a)^1(52a)^2(53a)^2(54a)^2$	0.85	0.87		0.86	
$\tilde{D}^2A$	$(49a)^2(50a)^1(51a)^2(52a)^2(53a)^2(54a)^2$	2.43	3.40		3.30	

[a] Ref. [18]. [b] Used as reference.

Table 5. Main geometrical parameters of the equilibrium molecular structure of the [δ-valerolactam]$_2$ dimer and of its cation in their electronic ground states. These parameters are computed at the DFT PBE0/aug-cc-pVDZ level of theory. Distances are in pm and angles in degrees. The not-shown parameters are close to those given in ref. [9].

	[δ-Valerolactam]$_2$	[δ-Valerolactam]$_2^+$
C_1–N_2	134.1	136.0
C_4–N_2	145.2	144.4
C_{19}–N_{18}	134.2	136.0
O_{24}–H_{16}	179.2 183.8[a]	170.4
C_1–O_3–H_{17}	121.3	129.9
C_{11}–C_1–N_2–C_4	4.9	1.5
C_1–N_2–C_4–C_5	21.5	16.3
C_1–N_2–C_4–H_{16}	174.5	178.0

[a] Ref. [9].

tion of the four lowest doublet electronic states of DHDB$^+$ (i.e. the $\tilde{X}$, $\tilde{A}$,$\tilde{B}$ and $\tilde{C}$ states). No resolved structures can be seen accordingly to the unfavorable Franck-Condon factors for the DHDB $\tilde{X}+h\nu \rightarrow$DHDB$^+$ ($\tilde{X}$, $\tilde{A}$, $\tilde{B}$, $\tilde{C}$)$+e^-$ ionization transitions and probably the congestion of the spectrum is due to overlapping between these vibronic bands. The ionization energy of DHDB is determined as IE (DHDB) $= 8.293 \pm 0.010$ eV, that is, 0.9 eV below the monomer IE, a very large shift due to the strong stabilization of the complex in its cationic form. For $h\nu > 9.3$ eV, the signal drops slowly towards the baseline. The origin of this signal decrease is multiple: i) close-to-zero Franck–Condon factors to populate the upper vibronic bands of DHDB$^+$ ($\tilde{X}$, $\tilde{A}$,$\tilde{B}$, $\tilde{C}$); ii) the absence of bound electronic states for internal energies between 1 and 2.4 eV; iii) the doublet states of DHDB$^+$ may undergo rapid intramolecular reactions and/or predissociation processes (see below); iv) vibrational excitation of the DHDB$^+$ following the dissociation of the dimer. No favorite mechanism can be given based on the present experimental data. Mechanism (iv) seems to be on action presently since the $[M+1]$ fragment dissociates in the spectrometer and it appears below the IE of the monomer.

c. Unimolecular Decomposition of the [δ-Valerolactam]$_2^+$ Cation

The lowest dissociation channels of the DHDB$^+$ and of the SHDB$^+$ dimers[38] are (energies computed at the PBE0/aug-cc-pVDZ including zero point energy correction and given with respect to the ground state of DHDB$^+$):

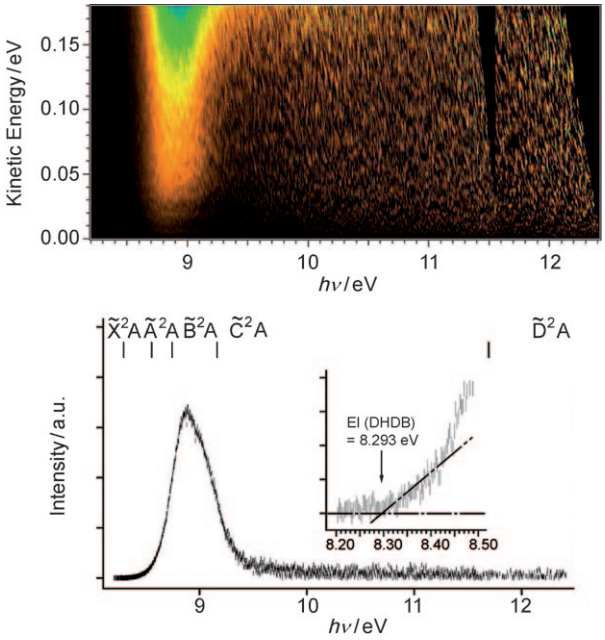

Figure 5. Top: Full-scale 2D spectrum of the (δ-valerolactam)$_2$ dimer providing the photoelectron kinetic energies as a function of the photon energy after the energy-shifting and mass-selecting treatment. Bottom: SPES for electron kinetic energies from 0 to 75 meV as deduced from the 2D spectrum. The positions of the theoretically determined origin transitions are highlighted with vertical bars (Table 4). The inset corresponds to an expansion of the DHDB photoionization threshold to determine the ionization energy (IE) of DHDB.

DL2 corresponds to the formation of the monomer and monomer cation from DHDB$^+$, whereas DL1 and DL3 represent the proton-transfer channel in addition to the dissociation. Since DL2 produces the monomer cation, M$^+$, as a fragment, it

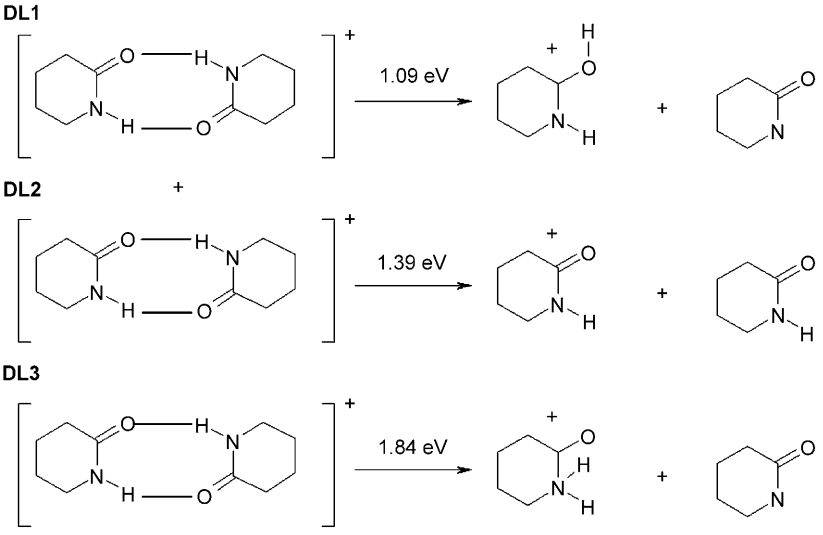

is difficult to extract it experimentally from the monomer's direct ionization. To verify its existence, we recorded six mass-selected ion images between 9 and 12 eV by merely changing the polarity on the spectrometer's electrodes. These images permit the differentiation of the direct and dissociative processes leading to the formation of M^+ by the measurement of the kinetic energy of the M^+ mass. The kinetic energy distributions at all six energies showed no trace of dissociative ionization. Unfortunately, we cannot definitely exclude the presence of DL2 since, at their first predicted appearance energy of 9.7 eV, the amount of direct dissociation of the monomer is huge, and would hide all the dissociative processes giving translational energies under 6 meV (70 K).

We do, however, observe the $(monomer+H)^+$, $(M+1)^+$, channel corresponding to DL1 and DL3, and this is shown in Figure 6 as a function of the photon energy. There are two clear rises in the image for which we can linearly extrapolate their onsets to obtain their appearance energies, which are measured to be 8.99 ± 0.02 and 10.82 ± 0.02 eV, that is, 0.7 and 2.53 eV above the dimer's first IE determined presently. Although the agreement with the theoretical PBE0/aug-cc-pVDZ values is far from perfect, the two dissociation channels DL1 and DL3 are separated enough as to prevent any ambiguity in the assignment. We thus assign an appearance energy of 8.99 eV to the DL1 and 10.82 eV to the DL3.

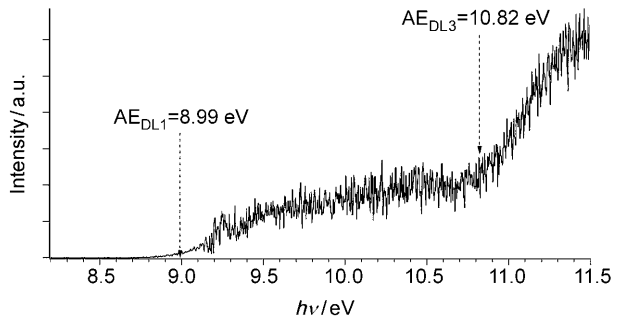

Figure 6. SPES for electron kinetic energies from 0 to 75 meV corresponding to the $(M+1)^+$ fragment. The two appearance thresholds correlate to the DL1 and DL3 $[\delta\text{-valerolactam}]_2^+$ dimer dissociation pathways (see text for details).

Since the lowest dissociation channel is DL1, that is, it includes a unique proton transfer, the dissociation of $DHDB^+$ occurs after opening of one of the double H bonds: the $SDHD^+$ structure is formed and involved during these complex dynamics. For interpretation, we present, in Figure 7, the CASSCF/aug-cc-pVDZ one-dimensional cuts of the potential energy surfaces of the lowest doublet electronic states of $(SHDB)^+$ along the dissociation coordinate (d coordinate) and along the intramolecular H-transfer coordinate. Figure 7C clearly shows that $SHDB^+$ isomerizes to give the more stable species $SHDB^+$, with both H on the same moiety, prior to dissociating into $(M+1)^+$ via the local minima at the right side of this figure. This occurs either in the ground state PESs or on the electronically excited PESs.

A coordinate relaxation is expected along the dissociation channel. Indeed, the cuts of Figure 7A do not converge adiabatically to the DL1 energies because the internal coordinates are fixed at their equilibrium values in $SHDB^+$, which are quite different for the fragments of DL1. Instead, the cuts of Figure 7B, at least for $SHDB^+$ $\tilde{X}^2A$, match quite well the fragments energies at large internuclear distances but they are far from reality in the molecular region. The minimal energy path for such reactions should be in between as we recently showed for other ion-molecule reactions smaller molecular systems.[39–42]

Accordingly, we propose the following mechanism: First, $DHDB^+$, either in its electronic ground state or electronically excited, is formed after photoionizing the neutral DHDB. Second, the most stable form of the dimer ion, that is, $SHDB^+$, is formed after intramolecular isomerization processes. Third, a proton transfer occurs where the H involved in the H bond (i.e. H_{16}, Figure 1) is transferred from N (N_2, Figure 1) of one moiety to O (O_{24}, Figure 1) of the other moiety. Finally, dissociation takes place to form $[monomer+H]^+$ and a priori [Monomer-H] species (DL1). Hence, the electronic states of the $dimer^+$ should undergo rapid (pre)dissociation processes shortening their lifetimes. For upper energies, additional processes may contribute such as H loss from the dimer cations or formation of the fragments in higher spin-multiplicities (cf. ref. [38] for more details).

4. Conclusion

We have studied the single-photon ionization of gas-phase δ-valerolactam and of its dimer by means of mass-selected veloc-

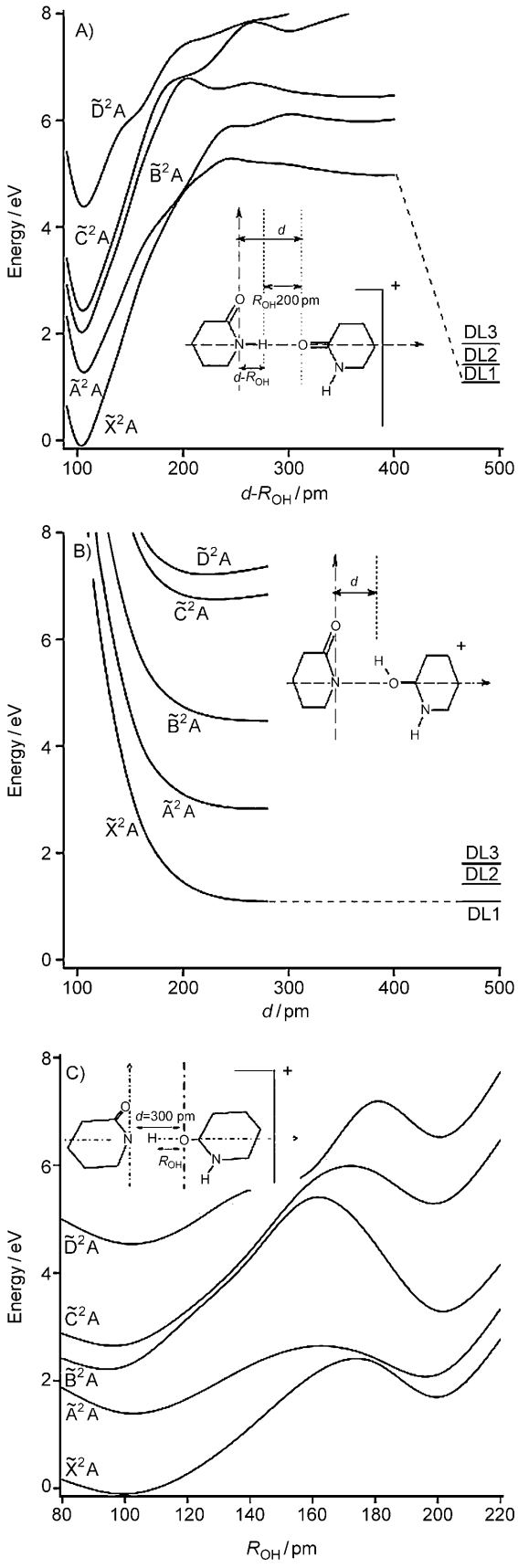

ity map imaging electron/ion spectroscopy coupled to VUV synchrotron radiation. For the monomer, the experimental spectra are rather well structured. We deduce the IEs of the [δ-valerolactam]$^+$ bands which are attributed to the population of some identified vibrational progressions of [δ-valerolactam]$^+$ in its electronic ground and excited states. Our work represents the first experimental determinations of the vibrational structure of [δ-valerolactam]$^+$. For the dimer, a large band extending over ~1 eV, is observed. It corresponds to the population of the four lowest electronic states of the [δ-valerolactam]$_2^+$ dimer. Above 0.7 eV from the IE threshold, the dimer dissociates to form the protonated monomer $(M+1)^+$. The interpretation of the experimental ionization spectra is performed with the help of the theoretical data. They concern the electronic structures (equilibrium geometries) and the vibrational spectra (harmonic and anharmonic wavenumbers) of the monomeric and dimeric cationic species. Our experimental and theoretical data compare quite well. Finally, the contribution of auto-ionization processes is surprisingly limited, at least close to the IEs, where direct photoionization seems to be dominant.

Acknowledgements

We are indebted to the general technical staff of Synchrotron Soleil for the operation of the facility. We would like also to thank Jean-François Gil for his technical help on the SAPHIRS molecular beam chamber. We thank J. C. Poully and C. Desfrançois for their help. A.M. would like to thank C. Soize for financial support.

Keywords: δ-valerolactam · dimers · ionization · photoelectron spectroscopy · vibrational transitions

[1] S. Ramaswamy, M. Scholze, B. V. Plapp, *Biochemistry* **1997**, *36*, 3522.
[2] T. H. Stanley, *J. Pain Symptom Manage.* **1992**, *7*, S3–7; DOI: 10.1016/0885-3924(92)90047L.
[3] M. R. Nimlos, D. F. Kelley, E. R. Bernstein, *J. Phys. Chem.* **1989**, *93*, 643.
[4] A. Warshel, M. Levitt, S. Lifson, *J. Mol. Spectrosc.* **1970**, *33*, 84.
[5] M. Rey-Lafon, M. T. Forel, C. Garrigou-Lagrange, *Spectrochim. Acta Part A* **1973**, *29*, 471.
[6] N. Kuze, H. Funahashi, M. Ogawa, H. Tajiri, Y. Ohta, T. Usami, T. Sakaizumi, O. Ohashi, *J. Mol. Spectrosc.* **1999**, *198*, 381.
[7] L. Treschanke, P. Rademacher, *J. Mol. Struct.: THEOCHEM* **1985**, *122*, 35.
[8] A. S. Edison, F. Weinhold, J. L. Markley, *J. Am. Chem. Soc.* **1995**, *117*, 9619.
[9] P. Pandey, A. K. Samanta, B. Bandyopadhyay, T. Chakraborty, *J. Mol. Struct.* **2010**, *975*, 343.

Figure 7. CASSCF/aug-cc-pVDZ one-dimensional cuts of the potential energy surfaces of the lowest doublet electronic states of $(SHDB)^+$ along the *d* coordinate (in A and B) and the proton transfer R_{OH} coordinate (in C). In A, $R_{OH}=200$ pm, the remaining internal coordinates are kept fixed at their equilibrium values in the $SHDB^+$ ground state. In B, $R_{OH}=100$ pm, the remaining internal coordinates are kept fixed at their equilibrium values in the fragments of $SHDB^+$ in their ground states (cf. ref. [38]). In C, we used the same conditions as for A but *d* was fixed to 300 pm and we varied the intermolecular R_{OH} distance. These curves are given in energy with respect to the energy of $DHDB^+$ at equilibrium. DL1, DL2 and DL3 are the three lowest dissociation limits of the dimer cation. See text for more details.

[10] M. Tsuboi, *Bull. Chem. Soc. Jpn.* **1951**, *24*, 75.
[11] H. Susi, J. S. Ard, *Arch. Biochem. Biophys.* **1966**, *117*, 147.
[12] J. M. Purcell, H. Susi, J. R. Cavanaugh, *Can. J. Chem.* **1969**, *47*, 3655.
[13] C. Y. S. Chen, C. A. Swenson, *J. Phys. Chem.* **1969**, *73*, 1363.
[14] P. Carmona, *Spectrosc. Lett.* **1986**, *19*, 495.
[15] M. Adler, B. Laughlin, S. G. Lieb, *Phys. Chem. Chem. Phys.* **1999**, *1*, 5333.
[16] N. A. Prokopenko, I. A. Bethea, C. J. Clemens IV, A. Klimek, K. Wargo, C. Spivey, K. Waziri, A. Grushow, *Phys. Chem. Chem. Phys.* **2002**, *4*, 490.
[17] V. K. Potapov, A. D. Filyugina, D. N. Shigorin, G. A. Ozerova, *Dokl. Akad. Nauk SSSR* **1968**, *180*, 398.
[18] L. Treschanke, P. Rademacher, *J. Mol. Struct.* **1985**, *122*, 47.
[19] http://www.synchrotron-soleil.fr/portal/page/portal/Recherche/LignesLumiere/DESIRS.
[20] B. Mercier, M. Compin, C. Prevost, G. Bellec, R. Thissen, O. Dutuit, L. Nahon, *J. Vac. Sci. Technol. A* **2000**, *18*, 2533.
[21] K. Yoshino, Y. Tanaka, *J. Opt. Soc. Am.* **1979**, *69*, 159.
[22] G. A. Garcia, H. Soldi-Lose, L. Nahon, *Rev. Sci. Instrum.* **2009**, *80*, 023102.
[23] G. A. Garcia, L. Nahon, C. J. Harding, E. A. Mikajlo, I. Powis, *Rev. Sci. Instrum.* **2005**, *76*, 053302.
[24] J. C. Poully, J. P. Schermann, N. Nieuwjaer, F. Lecomte G. Grégoire, C. Desfrançois, G. A. Garcia, L. Nahon, D. Nandi, L. Poisson, M. Hochlaf, *Phys. Chem. Chem. Phys.* **2010**, *12*, 3566.
[25] http://www.molpro.net.
[26] Gaussian 09 (Revision A.1), M. J. Frisch, G. W. Trucks, H. B. Schlegel, G. E. Scuseria, M. A. Robb, J. R. Cheeseman, G. Scalmani, V. Barone, B. Mennucci, G. A. Petersson, H. Nakatsuji, M. Caricato, X. Li, H. P. Hratchian, A. F. Izmaylov, J. Bloino, G. Zheng, J. L. Sonnenberg, M. Hada, M. Ehara, K. Toyota, R. Fukuda, J. Hasegawa, M. Ishida, T. Nakajima, Y. Honda, O. Kitao, H. Nakai, T. Vreven, J. A. Montgomery, Jr., J. E. Peralta, F. Ogliaro, M. Bearpark, J. J. Heyd, E. Brothers, K. N. Kudin, V. N. Staroverov, R. Kobayashi, J. Normand, K. Raghavachari, A. Rendell, J. C. Burant, S. S. Iyengar, J. Tomasi, M. Cossi, N. Rega, N. J. Millam, M. Klene, J. E. Knox, J. B. Cross, V. Bakken, C. Adamo, J. Jaramillo, R. Gomperts, R. E. Stratmann, O. Yazyev, A. J. Austin, R. Cammi, C. Pomelli, J. W. Ochterski, R. L. Martin, K. Morokuma, V. G. Zakrzewski, G. A. Voth, P. Salvador, J. J. Dannenberg, S. Dapprich, A. D. Daniels, Ö. Farkas, J. B. Foresman, J. V. Ortiz, J. Cioslowski, D. J. Fox, Gaussian, Inc., Wallingford, CT, **2009**.
[27] T. H. Dunning, *J. Chem. Phys.* **1989**, *90*, 1007.
[28] D. E. Woon, T. H. Dunning, *J. Chem. Phys.* **1993**, *98*, 1358.
[29] C. Adamo, V. Barone, *J. Chem. Phys.* **1999**, *110*, 6158.
[30] R. E. Stratmann, G. E. Scuseria, M. J. Frisch, *J. Chem. Phys.* **1998**, *109*, 8128.
[31] D. Hammoutène, M. Hochlaf, I. Ciofini, C. Adamo, *Int. J. Quantum Chem.* **2010**, *110*, 498.
[32] P. J. Knowles, H.-J. Werner, *Chem. Phys. Lett.* **1985**, *115*, 259.
[33] H.-J. Werner, P. J. Knowles, *J. Chem. Phys.* **1985**, *82*, 5053.
[34] H.-J. Werner, P. J. Knowles, *J. Chem. Phys.* **1988**, *89*, 5803.
[35] P. J. Knowles, H.-J. Werner, *Chem. Phys. Lett.* **1988**, *145*, 514.
[36] G. A. Garcia, L. Nahon, I. Powis, *Rev. Sci. Instrum.* **2004**, *75*, 4989.
[37] M. Hochlaf, K.-M. Weitzel, C. Y. Ng, *J. Chem. Phys.* **2004**, *120*, 6944.
[38] Supplementary material contains the full set of the equilibrium geometries, harmonic wavenumbers and rotational constants of the dimers. We give also the lowest dissociation channels of $SHDB^+$.
[39] H. Ndome, M. Hochlaf, *Phys. Chem. Chem. Phys.* **2005**, *7*, 1568.
[40] H. Ndome, C. Alcaraz, M. Hochlaf, *J. Chem. Phys.* **2007**, *127*, 064312.
[41] H. Ndome, C. Alcaraz, M. Hochlaf, *J. Chem. Phys.* **2007**, *127*, 064313.
[42] H. Ndome, M. Hochlaf, *J. Chem. Phys.* **2009**, *130*, 204301.

Received: February 2, 2011
Published online on May 25, 2011

